AIAA SciTech Forum
23-27 January 2023, National Harbor, MD & Online
AIAA SCITECH 2023 Forum

10.2514/6.2023-1857

Numerical investigation of high-pressure transcritical shock-droplet interaction and mixing layer using VLE-based CFD accelerated by ISAT

Hongyuan Zhang* and Suo Yang†
Department of Mechanical Engineering, University of Minnesota – Twin Cities, Minneapolis, MN 55455, USA

To achieve high power density and thermodynamic cycle efficiency, the working pressures of liquid-propellant rocket engines, diesel engines, and gas turbines (based on deflagration or detonation) are continuously increasing, which could reach or go beyond the thermodynamic critical pressure of the liquid propellant. For this reason, the studies of trans- and super-critical injection are getting more and more attention. However, the simulation of transcritical phase change is still a challenging topic. The phase boundary, especially near the mixture critical point, needs to be accurately determined to investigate the multicomponent effects on transcritical injection and atomization. This work used our previously developed thermodynamic model based on the vapor-liquid equilibrium (VLE) theory, which can predict the phase separation near the mixture critical point. An *in situ* adaptive tabulation (ISAT) method was developed to accelerate the computationally expensive multicomponent VLE computation such that it can be cheap enough for CFD. The new thermodynamic model was integrated into OpenFOAM to develop a VLE-based CFD solver. In this work, shock-droplet interaction and two-phase mixing simulations are conducted using our new VLE-based CFD solver. The shock-droplet interaction simulation results capture the thermodynamic condition of the surface entering the supercritical state after shock passes through. The atomization of droplets could be triggered by vorticity formed at the droplets' surface. 2D temporal mixing layer simulations show the evolution of the transcritical mixing layer and capture the phase split effect at the mixing layer.

I. Introduction

The demand for high-performance combustors increases the chamber pressure continuously, which makes the working condition of some high-pressure combustors overlap with the supercritical region of fuel and/or oxidizer. The injection and mixing process is very different between subcritical and supercritical conditions [1, 2], which could affect the cold ignition in combustors. To understand the subcritical and supercritical mixing process, a simulation tool is needed. Since supercritical region is far from the ideal gas region, real-gas effect needs to be considered to capture correct behavior. In addition, transcritical and supercritical fluid behavior can be peculiar because of the large variation of thermophysical properties such as density and specific heat near the critical point. As a result, the Computational Fluid Dynamics (CFD) modeling of supercritical flows is very challenging. Since small changes in temperature and pressure can have large effects on the structure of a fluid near the critical point, local properties are very important. Furthermore, a supercritical fluid lacks surface tension, which means the modeling transcritical flow needs to capture the surface tension change when the fluid goes across phase boundary. This makes simulation of transcritical flow more challenging than supercritical flow.

The studies of transcritical and supercritical injection and mixing have attracted much interest in the past 30 years. However, most of them were mainly concentrated on single component system, whose critical point is a constant value. As long as the fluid exceeds itself critical point, it goes into the supercritical state, and the classical "dense-fluid" approach is used with the assumption of a single-phase [3]. Since the real mixture critical pressure could be significantly higher than the critical pressure of each component [4], the accurate mixture critical point needs to be obtained.

Recently, some works focus on the simulation of multicomponent transcritical flow, capturing the phase separation at high pressure. To capture phase separation, most works use the vapor-liquid equilibrium (VLE) theory. Yao, et al. developed a fluids solver based on VLE to investigate the impact of diffusion models of a laminar counterflow flame at

*Ph.D. Candidate, Student Member AIAA.
†Richard & Barbara Nelson Assistant Professor, suo-yang@umn.edu (Corresponding Author), Senior Member AIAA.

trans and supercritical conditions [5]. In Ray's work, VLE theory is used to understand fuel droplets evaporation at high pressures [6]. A similar framework is also used in P. Tudisco's works to understand the effect of Lewis number [7].

The VLE solver brings huge amount of computation cost, which limits the simulation of complex geometry, and multicomponent flow. To reduce the computational cost, Tudisco, et al. interpolate the thermodynamic properties from cell-centers to cell-interfaces [8], but still can not accelerate the computation at cell-centers. We tried to use a tabulation method to avoid computing of VLE model in our previous work [9]. However, the table size grows exponentially (table size M^N, M is the number of grids in the table; N is the number of components). For a flow with 4 components, table size will need several Terabytes, which makes this method completely unsuitable for combustion and many other practical problems.

In this work, we coupled *In Situ* Adaptive Tabulation (ISAT) with the transcritical fluid solver [10], to accelerate computation. Due to the ISAT method constructing the table during the computation, it only stores the necessary data, which only requires a small amount of computer storage, and achieves high computational speed [11]. The new solver with ISAT gained a great computational speed improvement. Simulations are conducted using our new VLE-based CFD solver to reveal the phase change effects on transcritical shock-droplet interaction and two-phase mixing.

II. Numerical Modeling

A. Models of thermodynamic and transport properties

This study uses VLE solvers to capture the phase change and determine the multicomponent mixture's critical point in the transcritical flow. VLE describes the phase equilibrium between liquid and vapor phases. Solving the set of VLE equations gives the phase fraction and compositions in the two phases. If the gas mole fraction (i.e., the mole fraction of vapor phase) is equal to 1 or 0, then the system is in a single phase. If the system falls into the two-phase region, the gas phase mole fraction will be between 0 and 1, and equilibrium between vapor and liquid phase is established. Three VLE solvers are implemented: TP flash, PV flash, and UV flash. TP flash solves VLE problems with a given temperature (T) and pressure (P), and is used for the first step update in fluid solver; PV flash solves problems with given pressure and specific volume (V), and is used for double flux scheme update; UV flash solves problems with given internal energy (U) and specific volume (V), and is for a fully-conservative scheme.

Isothermal and isobaric (TP) flash: VLE is governed by fugacity equality Eq. (1) and Rachford-Rice equation [12] Eq. (2), which is an additional constraint to the equilibrium solver as used in Saha and Carroll [13] and obtained from the conservation of each component.

$$f_{i,l} \big/ f_{i,g} = 1 \tag{1}$$

$$\sum_{i=1}^{N} \left\{ z_i \left(1 - K_i\right) \Big/ \left[1 + \left(K_i - 1\right) \psi_g\right] \right\} = 0 \tag{2}$$

$$K_i = y_i / x_i \tag{3}$$

$$\sum_{i=1}^{N} x_i = \sum_{i=1}^{N} y_i = 1 \tag{4}$$

where $f_{i,p}$ is the fugacity of component i in phase p ($p = l$: liquid; $p = g$: gas), x_i is the mole fraction of component i in liquid phase, y_i is the mole fraction of component i in gas phase, z_i is the mole fraction of component i in the feed (i.e., the whole mixture including both gas phase and liquid phase), ψ_g is the gas mole fraction, K_i is the equilibrium constant of component i.

The real fluid properties are described using the Peng-Robinson equation of state (PR-EOS) [14] as:

$$P = \frac{RT}{V - b} - \frac{a}{V\left(V + b\right) + b\left(V - b\right)} \tag{5}$$

where P, R, T and V are pressure, gas constant, temperature, and specific volume respectively. For single-component fluid, the PR-EOS parameters are given by

$$a = 0.45724 \frac{R^2 T_c^2}{p_c} \hat{a}, \qquad b = 0.07780 \frac{R T_c}{p_c}, \tag{6}$$

$$\hat{a} = \left(1 + \kappa \left(1 - \left(T_r\right)^{1/2}\right)\right)^2, \qquad \kappa = 0.37464 + 1.54226\omega - 0.26992\omega^2 \tag{7}$$

where subscript "c" means critical value, subscript "r" means the reduced value (e.g., $T_r = T/T_c$), ω is acentric factor.

The mixture PR-EOS parameters are calculated from the corresponding single component coefficients a_i and b_i using the mixing rule [15]:

$$a = \sum_i \sum_j \chi_i \chi_j (1 - b_{ij}) \sqrt{a_i a_j} \tag{8}$$

$$b = \sum_i \chi_i b_i \tag{9}$$

where χ_i is the mole fraction of component i (for liquid, $\chi_i = x_i$; for gas phase, $\chi_i = y_i$), b_{ij} is a binary interaction parameter.

Liquid phase and gas phase are described by a separate multicomponent PR-EOS. Specific volume of each phase, V_p, is solved from PR-EOS. From this, the compressibility factor of each phase ($Z = PV/RT$) can also be obtained.

The fugacity formula of PR-EOS is shown below [16]:

$$f_i = P\chi_i \exp\left[\frac{B_i}{B_{mix}}(Z-1) - ln(Z - B_{mix}) - \frac{A_{mix}}{2\sqrt{2}B_{mix}}\left(\frac{2\sum_j x_j A_j}{A_{mix}} - \frac{B_i}{B_{mix}}\right) \times ln\left(\frac{Z + (1+\sqrt{2})B_{mix}}{Z + (1-\sqrt{2})B_{mix}}\right)\right] \tag{10}$$

where χ_i is the mole fraction of component i (for liquid, $\chi_i = x_i$; for gas phase, $\chi_i = y_i$),

$$A_i = \frac{a_i p}{R^2 T^2} \qquad B_i = \frac{b_i p}{RT} \tag{11}$$

$$A_{mix} = \sum_i \sum_j x_i x_j (1 - b_{ij}) \sqrt{A_i A_j} \qquad B_{mix} = \sum_i x_i B_i \tag{12}$$

The equation set Eq. (1-12) is solved based on Newton iteration method. The flow chart of TP flash is shown in Fig. 1. The initial guess is obtained using Wilson Equation [17]:

$$K_i = e^{5.373(1+\omega_i)(1-1/T_{r,i})}/P_{r,i} \tag{13}$$

where ω_i is the acentric factor of component i; $T_{r,i}$ and $P_{r,i}$ are the reduced temperature and reduced pressure of component i, respectively. Then, solving Rachford-Rice equation (i.e., Eq. 2) using Newton iteration method to get ψ_g. x_i and y_i can be obtained from Eqs. (3) and (4). The next step is to evaluate fugacity using the Eq. (10-12), and examine whether fugacity equilibrium (i.e., $f_{i,l} = f_{i,g}$) has been reached. If not, update K_i by $K_i = K_i \times f_{i,l}/f_{i,g}$ and go back to solve Rachford-Rice equation. When the error is less than a tolerance (i.e., the Newton iteration is converged), the solver will break the loop and output the solution.

PV flash and UV flash: PV flash and UV flash solvers are developed based on the TP flash. Both of them use iteration methods. Initial guesses are obtained from the previous time step. After several iterations, when the error is smaller than tolerance, the solver returns a solution.

In PV flash, since pressure is given as an input, only temperature needs to be solved. A secant method is used to avoid the expensive derivative computation. In UV flash, two variables (temperature and pressure) need to be solved simultaneously, and the secant method cannot be applied. A Newton-Raphson method is used to solve the UV flash problems. Jacobian matrix is obtained using the analytical framework published in [18].

Transport properties: To evaluate the dynamic viscosity and thermal conductivity under transcritical conditions, the dense fluid formulas [19] are used. This method gives accurate estimations of viscosity and thermal conductivity of polar, non-polar, and associating pure fluids and mixtures. Its dynamic viscosity and thermal conductivity have similar formula:

$$\lambda = \lambda_0 \lambda^* + \lambda_p \tag{14}$$

where λ represents dynamic viscosity or thermal conductivity. λ_0 is the gas property at low pressures. λ^* and λ_p are high pressure corrections. At high pressures, λ_p is the major contributing term comparing to $\lambda_0 \lambda^*$. On the other hand, at low pressures, λ^* is approaching unity and the λ_p term is negligible such that Eq. 14 reduces to λ_0. Hence, the transition between subcritical and supercritical is smoothly described by the model.

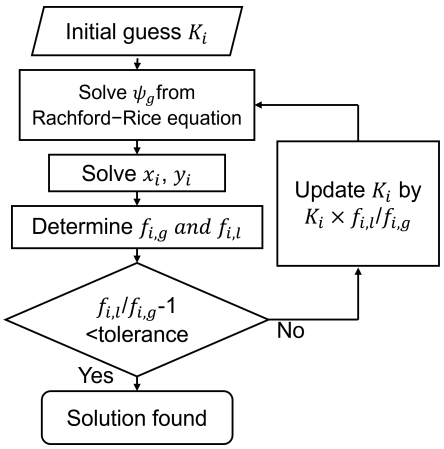

Fig. 1 Flow chart of TP flash solver.

B. *In Situ* Adaptive Tabulation (ISAT)

In situ adaptive tabulation method is introduced by Pope [11] to reduce the computational cost of detailed chemistry calculations. Comparing to the traditional tabulation methods which generate table before computation, ISAT dynamically constructs a table during the computation, which enable us to only store necessary record to reduce the table size. Although, ISAT still need to calculate the target function, most of queries can be directly retrieved by linear approximation. In addition, ISAT not only balances time and space cost, but also provides good error control. Hence, it is a good choice to accelerate the flash solvers.

The relation between the given condition and solution of flash solvers can be denoted as a function,

$$\boldsymbol{y = F\,(x)}$$

For every record in the table, it contains $(\mathbf{x}_0, \mathbf{y}_0, \left.\frac{\partial \mathbf{F}}{\partial \mathbf{x}}\right|_{\mathbf{x}_0}, \mathbf{M})$

The gradient, $\left.\frac{\partial \mathbf{F}}{\partial \mathbf{x}}\right|_{\mathbf{x}_0}$, is evaluated numerically and used for local linear approximation,

$$\mathbf{y}_{linear} = \mathbf{y}_0 + \left.\frac{\partial \mathbf{F}}{\partial \mathbf{x}}\right|_{\mathbf{x}_0} \cdot (\mathbf{x} - \mathbf{x}_0)$$

The matrix $\mathbf{M}$ is used to define the region of accuracy, in which the local error ϵ does not exceed the tolerance ϵ_{tol}. The region of accuracy is defined by inequality

$$(\mathbf{x} - \mathbf{x}_0)^T \mathbf{M}\,(\mathbf{x} - \mathbf{x}_0) \leq 1$$

The points satisfying this inequality is a hyper-ellipsoid. So, the region of accuracy is also called ellipsoid of accuracy (EOA).

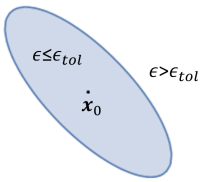

Fig. 2 Sketch of region of accuracy

For initial setting, the linear term is considered as error. So, the initial $\mathbf{M}$ can be set as

$$\mathbf{M} = \left(\left.\frac{\partial \mathbf{F}}{\partial \mathbf{x}}\right|_{\mathbf{x}_0}\right)^T \left(\left.\frac{\partial \mathbf{F}}{\partial \mathbf{x}}\right|_{\mathbf{x}_0}\right) / \epsilon_{tol}^2$$

.

For the first query, a new record calculated and added to table. For subsequent queries ($\mathbf{x}_{new}$), the closest record ($\mathbf{x}_0, \mathbf{y}_0, \left.\frac{\partial \mathbf{F}}{\partial \mathbf{x}}\right|_{\mathbf{x}_0}, \mathbf{M}$) is find out.

(1). **Retrieve**. If $\mathbf{x}_{new}$ is in the EOA of the record, then the linear approximation, $\mathbf{y}_{linear}$, is returned.

(2). **Growth**. If retrieve failed, then $\mathbf{y}_{new} = \mathbf{F}(\mathbf{x}_{new})$ is calculated. If $|\mathbf{y}_{new} - \mathbf{y}_{linear}| \leq \epsilon_{tol}$, the EOA is grown. The new EOA is the smallest ellipsoid covering old EOA and $\mathbf{x}_{new}$. $\mathbf{y}_{new}$ is returned.

(3). **Addition**. If growth also failed, then new record is added to the table, and $\mathbf{y}_{new}$ is returned.

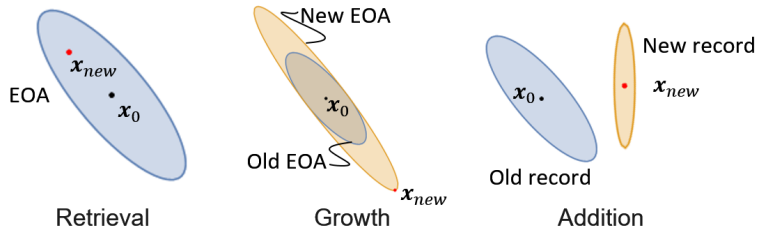

Fig. 3 Sketch showing the algorithm of ISAT method

C. CFD simulation framework

In this investigation, a transcritical multiphase CFD solver is developed by coupling a CFD solver with VLE solvers. The CFD solver is based on multicomponent transport equations, including the continuity equation, mixture momentum equations, mixture internal energy equation, and balance equations for distinct components in the mixture as follows:

$$\frac{\partial \rho}{\partial t} + \frac{\partial \rho u_i}{\partial x_i} = 0 \tag{15}$$

$$\frac{\partial \rho u_i}{\partial t} + \frac{\partial \rho u_i u_j}{\partial x_j} = \frac{\partial P}{\partial x_i} + \frac{\partial \tau_{ij}}{\partial x_j} \tag{16}$$

$$\frac{\partial \rho e}{\partial t} + \frac{\partial \rho u_i e}{\partial x_i} + \frac{\partial \rho K}{\partial t} + \frac{\partial \rho u_i K}{\partial x_i} + \frac{\partial u_i P}{\partial x_i} = -\frac{\partial q_i}{\partial x_i} + \frac{\partial \tau_{ij} u_j}{\partial x_i} \tag{17}$$

$$\frac{\partial \rho Y_m}{\partial t} + \frac{\partial \rho Y_m u_j}{\partial x_i} = \frac{\partial}{\partial x_j}\left(\rho D \sum_m h_m \frac{\partial Y_m}{\partial x_j}\right) \tag{18}$$

where ρ and e are mixture density and internal energy, respectively, and Y_m is mass fraction of component m.

The CFD solver is developed based on the central-upwind scheme [20]. The double-flux (DF) approach [21, 22] is used to mitigate the pressure fluctuations caused by real gas effect. At each time step, rho, u, and Y_i are updated using the central-upwind scheme. Then, the DF model is used to update e and p. After that, T, ψ_g, c are obtained using the ISAT PV flash solver. For the fully-conservative scheme (no DF method), p, T, ψ_g, c are directly updated using ISAT UV flash solver. This process is shown in Fig. 4.Double flux is import to solve the system with large density gradient, but since it's not an energy-conservative scheme, which could cause temperature overshoot. When the overshoot of temperature is unacceptable, a fully-conservative scheme is preferred.

III. Results, Analysis, and Discussion

A. 3D Transcritical Shock-Droplet Interaction

A test case is conducted on a three-dimensional domain and simulates the interaction between a shock wave and a droplet. The schematic of the 3D shock-droplet interaction is shown in Fig. 5. This test case is to study the multicomponent VLE effect as the thermodynamic state is suddenly changed by the shock. The domain size is 2L×L×L, $L = 1m$, and the uniform grid is discretized using 256×128×128 grid points. The initial droplet is placed at the center of the domain with a diameter $d = L/4$. The droplet is composed of C_6H_{14}. The surrounding environment is filled with to N_2 and H_2O (5% H_2O by mass). Water is added to represent impurities introduced from the previous combustion

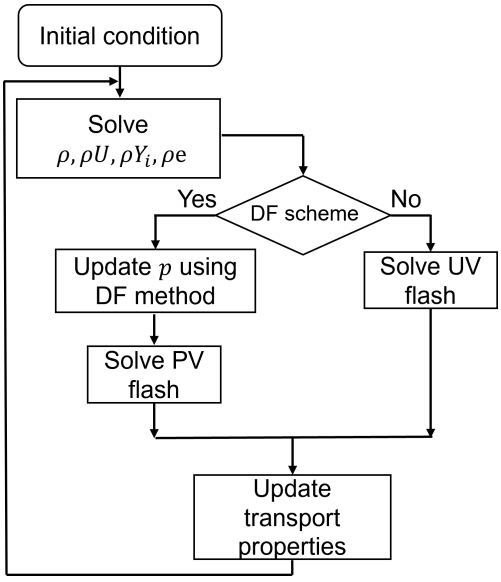

Fig. 4 Flow chart of the VLE-based CFD solver.

or surroundings. Since the critical pressure of water is very high, which could affect the thermodynamic properties significantly, we want to investigate its influence on droplet evaporation. A high-pressure region ($l = 3mm$) is set to generate a shock wave.

The initial state of the low-pressure region is set to $p = 20$ MPa, $T = 311$ K, $u = v = 0$, which is a VLE condition for this mixture. On the other hand, the high-pressure region is set to $p = 80$ MPa, $T = 311$ K, $u = v = 0$. Post-shock conditions are $p = 38$ MPa, $u = 154$ m/s and $T = 360$ K. This condition is expected to push the mixture into the supercritical region. The double flux method is used to conduct the simulation.

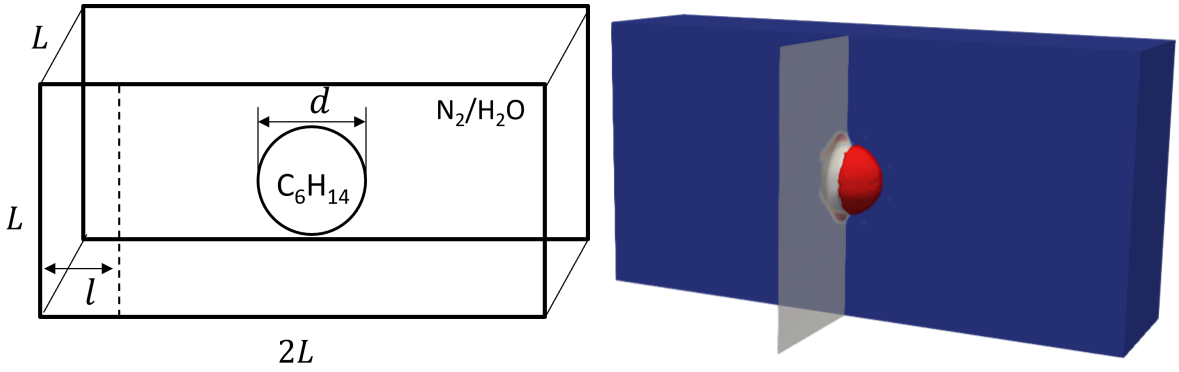

Fig. 5 Schematic of the 3D shock-droplet interaction. Left: relevant dimensions. Right: a snapshot of simulation results, the red isosurface: vapor fraction $\psi_g = 0.6$, white isosurface: mass fraction of C_6H_{14} $x_{C6H14} = 0.7$, transparent surface: shock front, 2D contour: vorticity magnitude. The right plot shows when shock travels through the droplet, the subcritical interface disappears, and vortex is generated at the droplet surface.

The contour plots of the pressure, mass fraction of C_6H_{14}, α, and vorticity magnitude are shown in Fig. 6 and Fig. 7. To better visualize the phase split, we define a new variable $\alpha = \psi_g(1 - \psi_g)$, which is zero in single-phase mixtures and reaches its maximum 0.25 at $\psi_g = 0.5$. The plots show that when shock-droplet interaction start, a reflect wave and a incident wave form. The reflection wave generates a high temperature and high pressure region in front of the droplets, which which evaporate the liquid water in the region. The incident wave is weaker than reflection wave. In addition, the surface of the droplet is under VLE condition. Due to the high pressure and temperature caused by shock, the state of interface enters the supercritical state (α drop to 0). When the shock pass through the droplets, the droplet is squeezed

horizontally, but no atomization happens. After the shock wave passes the droplet, vortex forms at the droplet surface, and it triggers the deformation of the droplet, which could cause the droplet atomization. The density outside of the droplets at four time instants are show in Fig. 8. The high-density region on the plots shows the evolution of reflection waves. Compared to the VLE results, the result without the VLE model underestimated density (7%, $28 kg/m^3$), which is because the VLE model captures water evaporation, and evaporation absorbs latent heat, causing lower temperature and higher density.

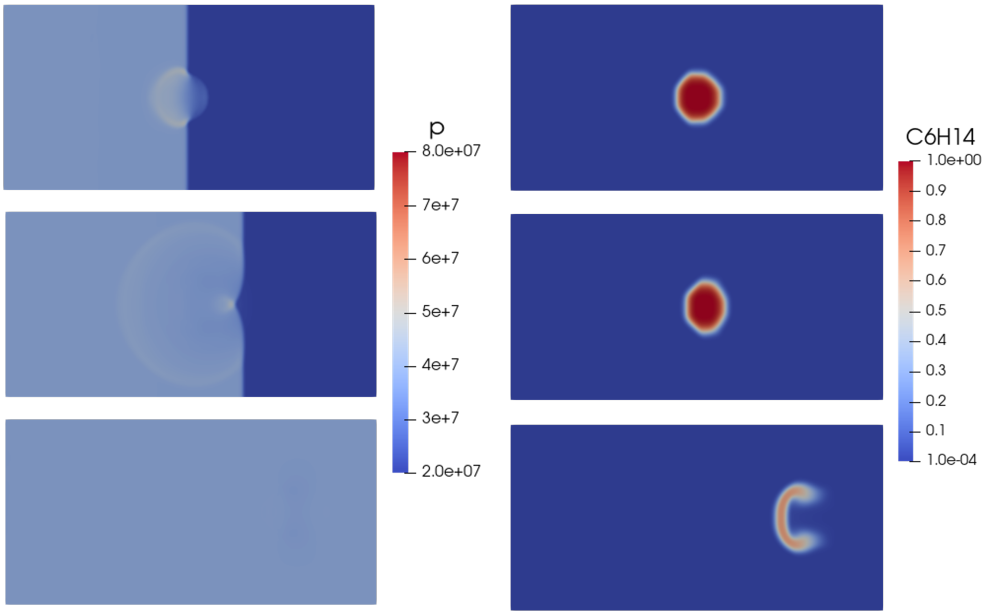

Fig. 6 Contour of pressure and mass fraction of C_6H_{14} at 1.31×10^{-5} (top), 1.87×10^{-5} (middle), 6.3×10^{-5} (bottom).

B. 2D Transcritical Two-Phase Mixing Layer

To investigate the mixing process in high-pressure flow, 2D temporal mixing layer simulations are conducted. The computation domain is shown in Fig 9. The domain is rectangular of size $L_x \times L_y$, and finer meshes are used in a rectangular subdomain of $L_x \times L_{TML}$, which is a uniformly discretized mesh with 64×128 cells. The top stream is filled with n-hexane at different temperatures, while the bottom stream is filled with nitrogen at a fixed temperature. For all three cases, the initial Reynolds number is fixed to 600, the nominal convective Mach number is fixed to 0.4 and the pressure is fixed to 5 MPa for all cases. The more initial conditions including initial mixing layer thickness δ, stream velocities, and domain sizes are given in are listed in Table 1. Other initialization follows Masi's approach in [23]. The fully-conservative method is used to conduct the simulations.

Table 1 Conditions for Case 1 to Case 3 for the Temporal Mixing Layer.

	T_T (K)	U_T (m/s)	U_B (m/s)	$L_x(m)$	δ(m)	T_T/T_c
Case 1	395	133.85	202.16	3.44×10^{-6}	8.6×10^{-7}	0.78
Case 2	545	79.59	102.34	3.70×10^{-6}	9.25×10^{-7}	1.07
Case 3	595	87.86	108.13	4.34×10^{-6}	1.08×10^{-6}	1.17

Subscripts T and B refer to "TOP" and "BOTTOM", respectively. For all three cases: p = 5MPa, T_B = 293.0K.

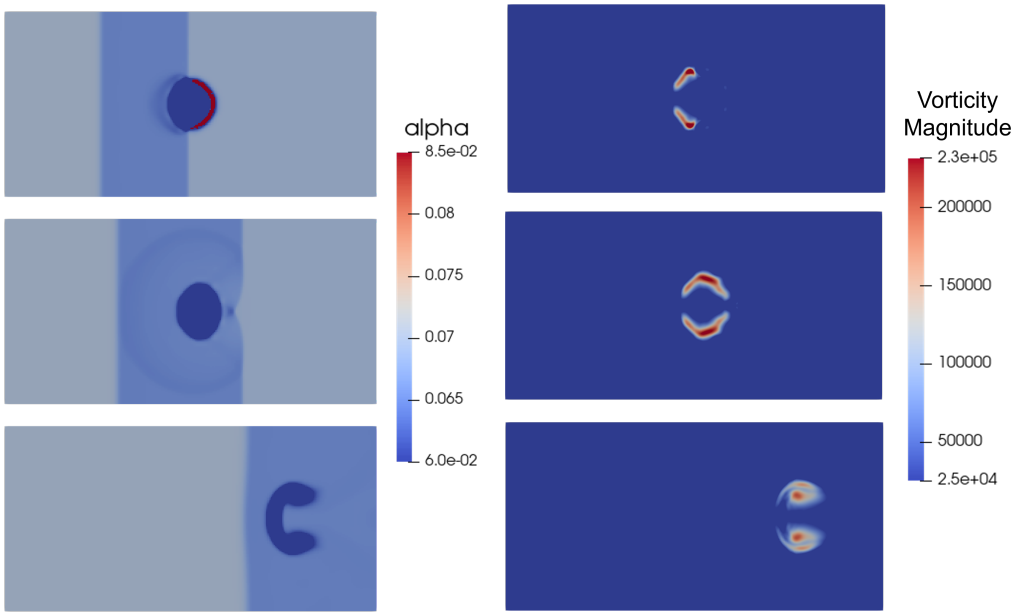

Fig. 7 Contour of α, and vorticity magnitude at 1.31×10^{-5} (top), 1.87×10^{-5} (middle), 6.3×10^{-5} (bottom).

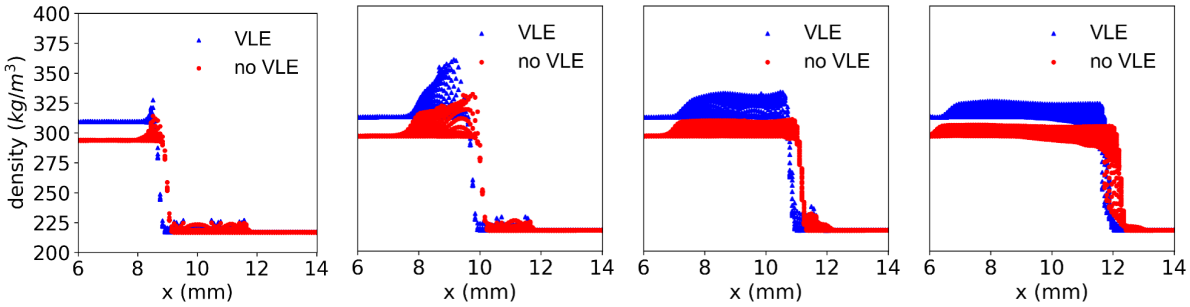

Fig. 8 Density plots of four time instants outside of the droplets.

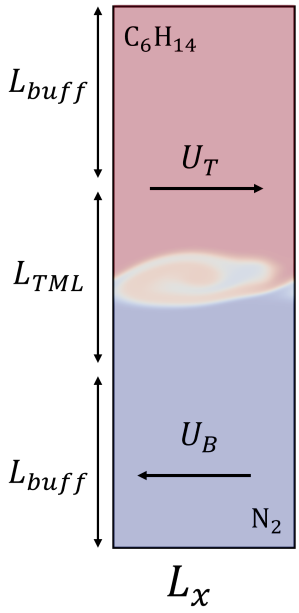

Fig. 9 Schematic of the 2D Temporal Mixing Layer

In case 1 results, Fig. 10, we can observe the process of TML evolution. The results start from a thin mixing layer (Fig. 10(a)), and then the initial perturbation in the velocity field triggers Kelvin–Helmholtz instability to grow (Fig. 10(b)). In Fig. 10(c), a vortex is formed in the mixing layer. After about $5 \times 10^{-8} s$, the vortex breaks down and forms smaller vortex(Fig. 10(d)), and finally, a thicker mixing layer is formed (Fig. 10(e)). The formation of the vortex and its breakdown happens in the early stage. After a thicker mixing layer is formed, the velocity and density gradient are greatly reduced, and Helmholtz instability is harder to grow.

Fig. 11 shows the phase split in the mixing layer for all three cases. In Case 1, strong phase split is observed, where α reaches its maximum 0.25. In Case 2, only moderate phase split is observed, where α ranges between 0 and 0.14. Finally, when C_6H_{14} temperature reaches 595, phase split is completely absent in Case 3.

We can see although the T_T/T_c in case 2 is larger than one, the mixing process causes the loss of C_6H_{14} internal energy and makes the phase split happen.

Conclusion

We implemented a vapor-liquid equilibrium (VLE) solvers and coupled them with a computational fluid dynamics (CFD) solver using the central-upwind scheme and double-flux method to capture the mixing and phase separation processes of mixtures. A shock-droplet interaction simulation is conducted. The simulation results capture the thermodynamic condition of the surface entering the supercritical state after shock passes through. The evaporation of liquid water in surrounding caused by reflection wave is also captured. At such transcritical conditions, the atomization of droplets could be triggered by vorticity formed at droplets' surface. 2D temporal mixing layer simulations show the evolution of the transcritical mixing layer, and capture the phase split effect at the mixing layer.

Acknowledgments

S. Yang gratefully acknowledges the support from the National Science Foundation (NSF) grant under Award No. CBET 2023932 and the Office of Naval Research (ONR) grant under Award No. N00014-22-1-2287 under the supervision of project monitor Dr. Steven Martens. H. Zhang gratefully acknowledges the support from the Frontera Computational Science Fellowship. The authors gratefully acknowledge the computing resources provided by the Minnesota Supercomputing Institute (MSI).

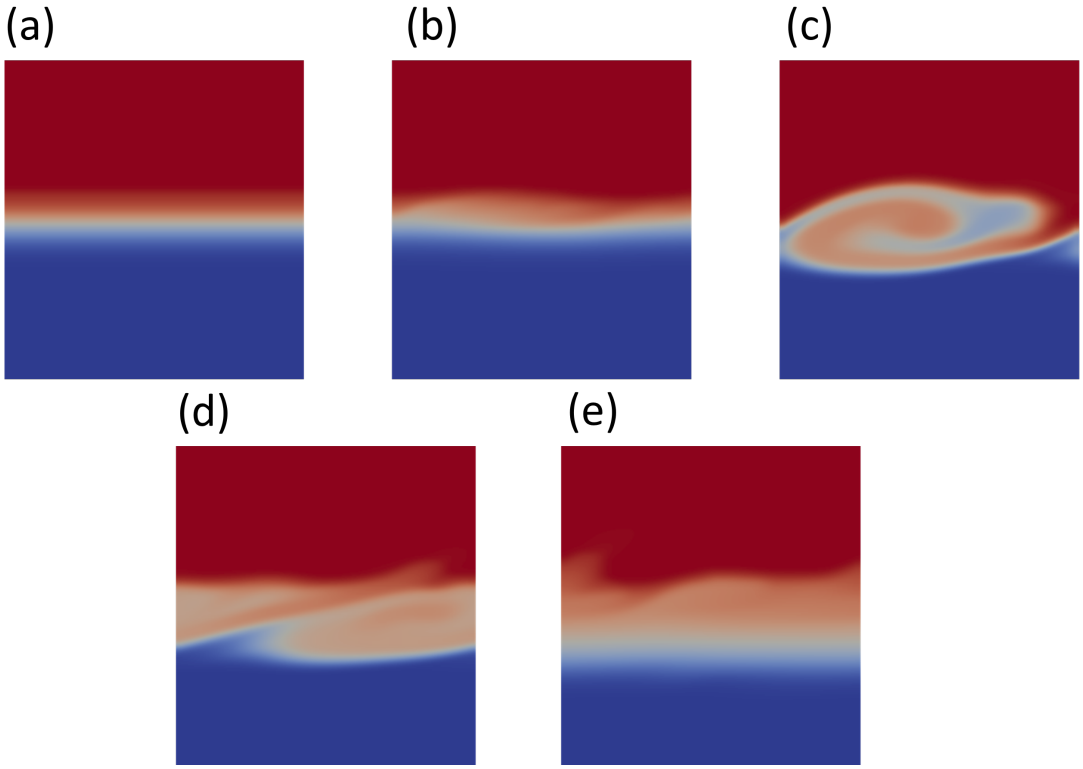

Fig. 10 The evolution of TML shown by C_6H_{14} mass fraction contour at different time instances of case 1: (a) 0, (b) $1 \times 10^{-7}s$, (c) $1.6 \times 10^{-7}s$, (d) $1.9 \times 10^{-7}s$, (e) $5 \times 10^{-7}s$.

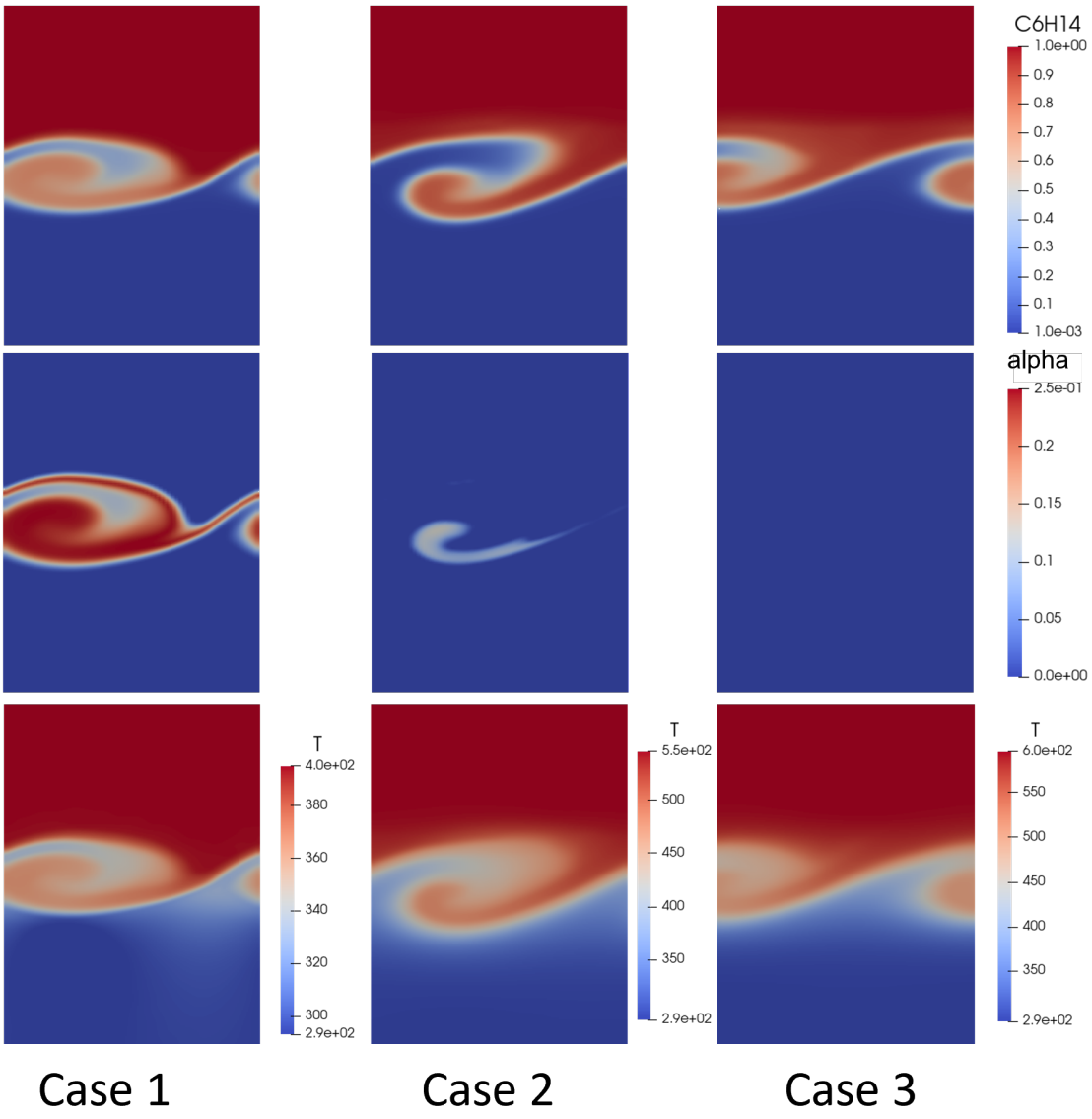

Fig. 11 The VLE effect in TML. Left, Case 1; middle, Case 2; right, Case 3. Top, mass fraction of C_6H_{14}; middle, α, $\alpha = \psi_g(1-\psi_g)$; bottom, temperature.

References

[1] Chehroudi, B., Talley, D., and Coy, E., "Initial growth rate and visual characteristics of a round jet into a sub-to supercritical environment of relevance to rocket, gas turbine, and diesel engines," *37th Aerospace Sciences Meeting and Exhibit*, 1999, p. 206.

[2] Mayer, W., and Smith, J. J., "Fundamentals of supercritical mixing and combustion of cryogenic propellants," *Liquid Rocket Thrust Chambers: Aspect of Modeling, Analysis, and Design, Progress in Astronautics and Aeronautics*, Vol. 200, 2004, pp. 339–368.

[3] Yang, V., "Modeling of supercritical vaporization, mixing, and combustion processes in liquid-fueled propulsion systems," *Proceedings of the Combustion Institute*, Vol. 28, No. 1, 2000, pp. 925–942.

[4] Van Konynenburg, P., and Scott, R., "Critical lines and phase equilibria in binary van der Waals mixtures," *Philosophical Transactions of the Royal Society of London. Series A, Mathematical and Physical Sciences*, Vol. 298, No. 1442, 1980, pp. 495–540.

[5] Yao, M. X., Hickey, J.-P., Ma, P. C., and Ihme, M., "Molecular diffusion and phase stability in high-pressure combustion," *Combustion and Flame*, Vol. 210, 2019, pp. 302–314.

[6] Ray, S., Raghavan, V., and Gogos, G., "Two-phase transient simulations of evaporation characteristics of two-component liquid fuel droplets at high pressures," *International Journal of Multiphase Flow*, Vol. 111, 2019, pp. 294–309.

[7] Tudisco, P., and Menon, S., "A vapor–liquid equilibrium induced Lewis number effect in real-gas shear layers: A theoretical study," *Physics of Fluids*, Vol. 32, No. 11, 2020, p. 112111.

[8] Tudisco, P., and Menon, S., "Numerical Investigations of Phase-Separation During Multi-Component Mixing at Super-Critical Conditions," *Flow, Turbulence and Combustion*, Vol. 104, No. 2, 2020, pp. 693–724.

[9] Zhang, H., Yi, P., and Yang, S., "Multicomponent Effects on the Supercritical CO2 Systems: Mixture Critical Point and Phase Separation," *Flow, Turbulence and Combustion*, Vol. 109, No. 2, 2022, pp. 515–543.

[10] Zhang, H., and Yang, S., "Multi-component transcritical flow simulation based on in situ adaptive tabulation of vapor-liquid equilibrium solutions," *AIAA Scitech 2021 Forum*, 2021, p. 0549.

[11] Pope, S. B., "Computationally efficient implementation of combustion chemistry using in situ adaptive tabulation," *Combustion Theory and Modelling*, Vol. 1, No. 1, 1997, pp. 41–63.

[12] Rachford Jr, H., Rice, J., et al., "Procedure for use of electronic digital computers in calculating flash vaporization hydrocarbon equilibrium," *Journal of Petroleum Technology*, Vol. 4, No. 10, 1952, pp. 19–3.

[13] Saha, S., and Carroll, J. J., "The isoenergetic-isochoric flash," *Fluid phase equilibria*, Vol. 138, No. 1-2, 1997, pp. 23–41.

[14] Peng, D.-Y., and Robinson, D. B., "A new two-constant equation of state," *Industrial & Engineering Chemistry Fundamentals*, Vol. 15, No. 1, 1976, pp. 59–64.

[15] Reid, R. C., Prausnitz, J. M., and Sherwood, T. K., *The Properties of Liquids and Gases.(Stichworte Teil 2)*, McGraw-Hill, 1977.

[16] Yi, P., Yang, S., Habchi, C., and Lugo, R., "A multicomponent real-fluid fully compressible four-equation model for two-phase flow with phase change," *Physics of Fluids*, Vol. 31, No. 2, 2019, p. 026102.

[17] Wilson, G. M., "Vapor-liquid equilibrium. XI. A new expression for the excess free energy of mixing," *Journal of the American Chemical Society*, Vol. 86, No. 2, 1964, pp. 127–130.

[18] Tudisco, P., and Menon, S., "Analytical framework for real-gas mixtures with phase-equilibrium thermodynamics," *The Journal of Supercritical Fluids*, Vol. 164, 2020, p. 104929.

[19] Chung, T. H., Ajlan, M., Lee, L. L., and Starling, K. E., "Generalized multiparameter correlation for nonpolar and polar fluid transport properties," *Industrial & engineering chemistry research*, Vol. 27, No. 4, 1988, pp. 671–679.

[20] Kurganov, A., Noelle, S., and Petrova, G., "Semidiscrete central-upwind schemes for hyperbolic conservation laws and Hamilton–Jacobi equations," *SIAM Journal on Scientific Computing*, Vol. 23, No. 3, 2001, pp. 707–740.

[21] Abgrall, R., and Karni, S., "Computations of compressible multifluids," *Journal of computational physics*, Vol. 169, No. 2, 2001, pp. 594–623.

[22] Billet, G., and Abgrall, R., "An adaptive shock-capturing algorithm for solving unsteady reactive flows," *Computers & fluids*, Vol. 32, No. 10, 2003, pp. 1473–1495.

[23] Masi, E., Bellan, J., Harstad, K. G., and Okong'o, N. A., "Multi-species turbulent mixing under supercritical-pressure conditions: modelling, direct numerical simulation and analysis revealing species spinodal decomposition," *Journal of Fluid Mechanics*, Vol. 721, 2013, pp. 578–626.